Soft x-ray ionization induced fragmentation of glycine

E. Itälä[a], K. Kooser[a], E. Rachlew[b], M. A. Huels[c], E. Kukk[a,d]

[a] *Dept. of Physics and Astronomy, University of Turku, FIN-20014 Turku, Finland*

[b] *Department of Physics, KTH, 10691 Stockholm, Sweden*

[c] *Department of Nuclear Medicine and Radiobiology, Facility of Medicine, University of Sherbrooke, Sherbrooke, JIH 5N4 Quebec, Canada*

[d] *Turku University Centre for Materials and Surfaces (MatSurf), FIN-20014 Turku, Finland*

Abstract

X-ray absorption commonly involves dissociative core ionization producing not only momentum correlated charged fragments but also low- and high-energy electrons capable of inducing damage in living tissue. This gives a natural motivation for studying the core ionization induced fragmentation processes in biologically important molecules such as amino acids. Here the fragmentation of amino acid glycine following carbon 1s core ionization has been studied. Using photoelectron-photoion-photoion coincidence (PEPIPICO) technique a detailed analysis on fragmentation of the sample molecule into pairs of momentum correlated cations has been carried out. The main characteristics of core ionization induced fragmentation of glycine were found to be the rupture of the C-C_α bond and the presence of the CNH_2^+ fragment.

I. INTRODUCTION

Ionizing radiation often causes destruction of the target molecule and irreversible damage when interacting with living cells. The primary damage is caused by photofragmentation that almost always follows atomic core ionization and electronic relaxation by Auger decay. We present here a study on fragmentation of core ionized gas phase glycine molecule. In living organisms glycine helps to create muscle tissue, convert glucose into energy and maintain healthy central nervous and digestive systems. Glycine is also widely used in different areas of industry; food, cosmetics, pharmaceuticals and fertilizers, to name few. While the biological significance of glycine is unquestionable, glycine (as well as the other amino acids) is also an interesting molecule from the viewpoint of astrochemistry. During the

past years several discoveries have been made concerning the existence of amino acids in space[1–3] and in 2009 NASA confirmed the first discovery of glycine in a comet. These discoveries have contributed to the discussion about the origins of life on Earth and sparked common interest in studying different biomolecules in space-like conditions[4–6].

Glycine (see Fig. 1), the simplest one of the 20 amino acids commonly found in proteins, has a zwitterionic character (positive and negative charge, located at the amino (NH_2) and the carboxyl (COOH) groups, respectively). However, this is only so in the condensed and liquid phase; in gas phase glycine appears as a neutral molecule where the charge is evenly distributed[7,8]. It is common for glycine to form hydrogen bond(s) between the -NH_2 group and the carbonyl (C=O) or the hydroxyl (-OH) group. Theoretical studies have predicted a number of different conformers[9–13], where (see Fig. 1) the -OH and -NH_2 groups are at the same or opposite side of the C-C_α bond on the plane of the atoms (excluding H). According to several references found in literature[11,13–15] the most stable geometry is where the -OH and -NH_2 groups are on opposite sides and where there is a bifurcated hydrogen bond between the amino group and the carbonyl group (Fig 1 (a)). The predicted abundancies for the confromers are 52.6% for (a), 9.0% for (b), 29.6% for (c) and 6.8% for (d)[15].

We investigated the fragmentation patterns of glycine dications that are created by the Auger decay process of core vacancies. Dissociation of the doubly charged molecule commonly creates two charged and a number of neutral fragments. The experimental method applied was electron energy resolved photoelectron-photoion-photoion coincidence spectroscopy (PEPIPICO)[16–19], which allows not only the detection of momentum-correlated ion pairs originating from the same ionization event, but also gives very detailed description of the dissociation process and determination of kinetic energy released in the process[20–22]. In order to resolve mass ambiguities, measurements with glycine where the C_α atom was replaced with ^{13}C were carried out. Previous studies concerning photon- or electron induced fragmentation of glycine have all concentrated on valence ionization[23–25], leaving core ionization induced fragmentation virtually unheeded. While the valence ionization is relevant when considering for example damage caused by ultra violet (UV) radiation, core-level ionization is the major channel in x-ray absorption. In addition to photons and electrons, also high-energy ions have been used to study the fragmentation of free and clustered glycine[26,27]. The fragmentation of glycine was found to be characterized by the rupture of the C-C_α bond leading to the creation of the CH_2NH_2 and COOH fragments regardless of the ionization technique. In the case of UV-radiation, electron- and He^{2+} impact ionization, the positive charge has a negligible probability (1-5%) to be localized to the COOH moiety[7,23,25,27]. In the case of Xe^{20+} bombardment, however, the probability for $COOH^+$ cation production increases significantly (up to ∼30%)[26]. Here we find that core ionization of glycine very often involves charge localization into

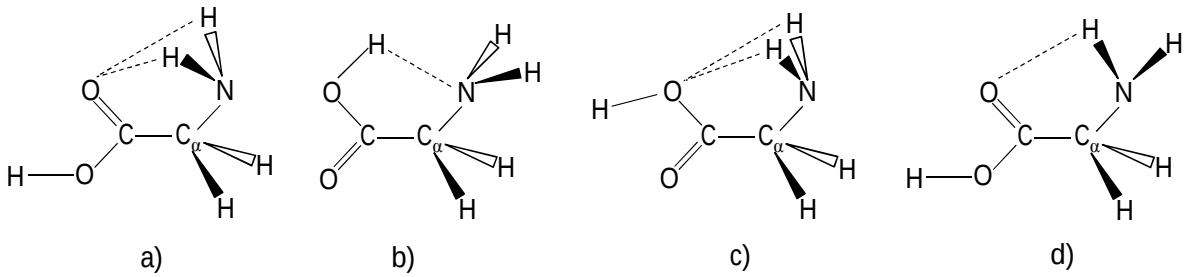

Figure 1: Four most common and stable conformers of glycine (NH_2CH_2COOH) molecule in the order of increasing energy. The dashed lines denote hydrogen bonding. In case of the isotopically labeled sample. the α-carbon was replaced with ^{13}C. The Figure is based on results on Refs.[11,13–15].

the COOH moiety.

II. EXPERIMENTAL

The apparatus and method for the present photoelectron-photoion-photoion coincidence (PEPIPICO) measurements has already been described in detail elsewhere[28], and only a brief summary is given here. The apparatus consists of a modified Scienta SES-100 electron energy analyzer[29], where the original CCD camera was replaced by a resistive anode detector (Quantar), and a home-made Wiley-Mclaren type ion time-of-flight detector with a 400 mm long drift tube. The ion spectrometer is equipped by 77 mm Hamamatsu MCP detector with the anode consisting of 10 concentric rings. The ion TOF is measured as the time difference from the fast preamplifier pulse from the electron detector and the recharge pulse of the ion MCP detector. The pulses from the 10 anode rings are delayed from 50

to 100 ns by 5 ns steps and can be used to determine the ion radial hit position, although this option was not used in the present experiment. The delay of triggering the ion extraction comprises of the electron transit time of about 150 ns and electronic delays. The ion detection electronics is based on a 1 GHz waveform digitizer card (Signatec PDA 1000). For the PEPIPICO measurements, the PEPICO system is operated in the pulsed extraction field mode and in the present experiment the extraction pulse voltage was ±156 V across the sample region, with the drift tube held at -850 V. The ion extraction pulses were triggered by the fast preamplifier signal from the electron detector. The samples were evaporated into the sample area using effusion cell with integrated cooling shroud (MBE Komponenten NTEZ40 oven) at around 145 °C.

The PEPIPICO data always contain some "false" coincidences of particles not originating from the same molecule. The probability of such events was kept small by using low counting rates < 20 electrons/s. In addition, artificial coincidence events were created during the measurement by a pulse generator so that two ion-ion coincidence maps were collected simultaneously – one in coincidence with electrons and one triggered by the pulse generator. The average number of ions per electron trigger was 0.9 and number of ions per artificial trigger 0.4 (including detector noise counts).

The ions were measured in coincidence with the C $1s$ photoelectrons at photon energy of 330 eV and using the electron kinetic energy window with range from 32 eV to 42 eV. The pass energy of the electron spectrometer was 100 eV and the entrance slit of the analyzer was 1.6 mm, which corresponds to the energy resolution of about 750 meV. Each PEPICO experiment monitors an energy window on the position sensitive electron detector that has a width of about 1/10th of the pass energy, while the resolution gives the accuracy of recording in each event the kinetic energy of the electrons that fall within this energy window. In post-experiment analysis, coincidence events can be selected from the full energy window or from a narrower electron energy subrange. In the present experiment, the full energy window was used for producing the coincidence maps. Higher resolution was not needed, since in this study it was only necessary to separate photoelectrons from different orbitals. The electron energy scale was calibrated by measuring Ar 2p photoline with various center energy values of the kinetic energy window of the electron detector keeping the photon energy at 280 eV. The center energy values were chosen for the Ar 2p photoline to be moved across the energy window by 1 eV steps. Using the measured electron hit coordinate values of the peak maxima, a dispersion curve $E_k(x)$ was made. The shift correction of the binding energy scale for the electron spectrum of glycine was done by using the C 1s binding energy of CO_2[30], which was visible in the C 1s spectrum of ^{13}C-glycine. Ion detection efficiency was about 30% accounting for grids and the MCP open area ratio. The collection efficiency

(transmission) is dependent on the ion velocity: according to our simulations, all heavy (M>2 amu) ions were collected in the coincidence events of our experiments, but significant losses can occur for fast hydrogen ions.

The experiment was performed at beamline I411 at MAX-II synchrotron radiation facility (Lund, Sweden)[31]. Undulator radiation was monochromatized using a modified Zeiss SX-700 monochromator. The samples were purchased from Sigma-Aldrich and were used "as is" with their stated purity being $\geq 99\%$.

III. RESULTS AND DISCUSSION

A. Classification and analysis methods

The analysis and fragment identification was done using so-called PEPIPICO maps, which represent the coincident fragment ion pairs as tilted patterns in the coordinate system of the ion time-of-flight (TOF) of the two detected fragments. Here the pattern's slope and length has been used to extract information about the fragmentation dynamics. Both the slope and the kinetic energy release (KER) were determined by rotating the PEPIPICO patterns in the (TOF1, TOF2) coordinates and then projecting the pattern down to x-axis (TOF1). The projection was fitted using a Gaussian function and the slope value was calculated from the rotation angle that gave the narrowest projection of the pattern. On the other hand, a rotation with the largest projection gave the length of the pattern which was used to determine the KER value. The error bars for the KER and slope values were determined using the standard deviations from fitting the narrowest and longest projections with model shapes.

More detailed slope analysis and KER determination methods in the context of PEPIPICO patterns are discussed in the Appendix and only a summary is given here. The general description for extracting the ion kinematics is described elsewhere[22,32], here we focus on extracting the fragmentation time sequences. Three basic sequential processes, namely *two-body* (a), *secondary decay* (b) and *deferred charge separation* (c) processes are often sufficient to describe and derive a great variety of many-body dissociation processes. Figure 2 illustrates the three basic processes (a, b, c) together with two processes derived from these (d, e). The time scale for the sequences of events for these processes lie in the order of few hundred femtoseconds[33], which is well below the time scale of the measurement (in the order of nanoseconds).

In two-body dissociation the two ions with charges q_1 and q_2 and masses M_1 and M_2 follow a strict momentum anti-correlation ($M_1 v_1 = -M_2 v_2$), which is seen as a tilted pattern of PEPIPICO events with the slope value of

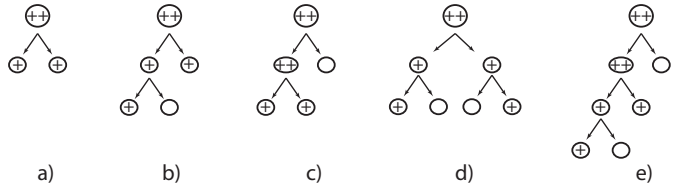

Figure 2: Fragmentation processes used to describe the dissociation processes of doubly charged glycine: two-body process (a), *secondary decay* (b), *deferred charge separation* (c), *two-step four-body secondary decay* (d) and *secondary decay* combined with *deferred charge separation* (e).

$k = -q_1/q_2$. For the two-body charge separation in molecular dication, $q_1 = q_2 = +e$ and $k = -1$. In a two-body dissociation the two momenta have equal magnitude p, in which case the length W (in time units) of the corresponding pattern in the PEPIPICO map can be shown to be:

$$W = \frac{\sqrt{8} \cdot s \cdot p}{q \cdot U}, \tag{1}$$

where s is the length of the extraction region and U is the voltage applied across the source region. The KER in the two-body breakup is then obtained as:

$$\mathrm{KER} = p^2\left(\frac{1}{2M_1} + \frac{1}{2M_2}\right). \tag{2}$$

We have used the above expression for KER also in the case of single-step many-body process, with the assumption that nearly all of the energy released in the charge separation step goes to the charged fragments. The *secondary decay*, *deferred charge separation* and *two-step four-body secondary decay* processes all give slightly different slope and KER equations, which are given in the Appendix.

The KER values can be used to estimate distances of the two positive charges from each other at the beginning of the charge separation. The most straightforward way to do this is to treat the positive charges as point charges. This might sound quite inaccurate or even flaw, since the Auger final state of the molecule right before the charge separation is a double valence hole state and the valence orbitals cover most of the molecule, not just a highly localized space. A delocalized charge distribution would thus be more accurate approach to the double valence hole state prior to charge separation. However, we have here treated the valence holes as point charges, mainly just to see, if such a simple model gives any reasonable estimation about the distances of the two positive charges/valence holes at the moment of charge separation. The distance R between the charges at the start of the Coulomb explosion can be

expressed as:

$$R[\text{Å}] = \frac{14.40}{\text{KER[eV]}}. \tag{3}$$

B. Fragmentation following core ionization

The C 1s photoelectron spectrum of glycine is presented in Fig. 3 and the PEPIPICO maps of glycine, where the ions are measured in coincidence with the C 1s photoelectrons are presented in Fig. 4. The assignments of both ionic fragments corresponding to the patterns in Fig. 4 (a) are presented in Table I together with experimental slope values of the corresponding PEPIPICO patterns. Because the two samples (regular and ^{13}C-labeled) were measured with different extraction and acceleration voltages, the flight times of the ions fragments having the same M/q ratio are not directly comparable. The relative intensities of the patterns, however, are. The patterns in Fig. 4 are those where the lighter coincident fragment's mass is larger than one amu (all masses given in amu from now on). Also ion pairs where the lighter fragment is H^+ were detected; these patterns are not shown in Fig. 4, but are discussed later in text.

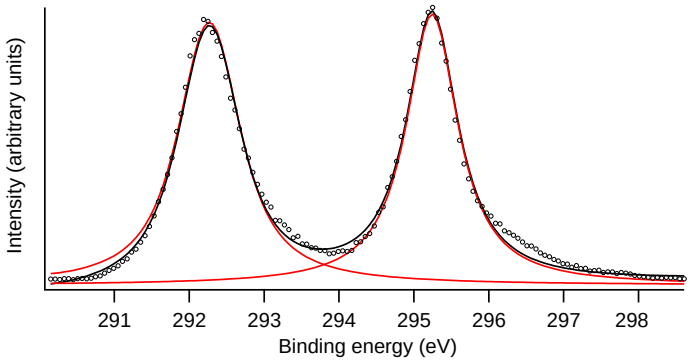

Figure 3: C 1s photoelectron spectrum of glycine. The high binding energy line belongs to the α carbon (see Fig. 1).

The photolines of Fig. 3 correspond to binding energies 295.3±0.1 eV and 292.3±0.1 eV, which is well in line with those in Ref.[34]. The clear separation of the two photolines makes it possible to also investigate if ionization site-specific fragmentation occurs. However, as in other cases before[35], no apparent site-specific effects were observed when coincidences with individual carbons were selected.

All the fragmentation processes of core ionized glycine corresponding to the patterns in Fig. 4 can be described quite well as a series of bond cleavages. The first step is most often either scission of the C-C$_\alpha$ bond or water elimination, as

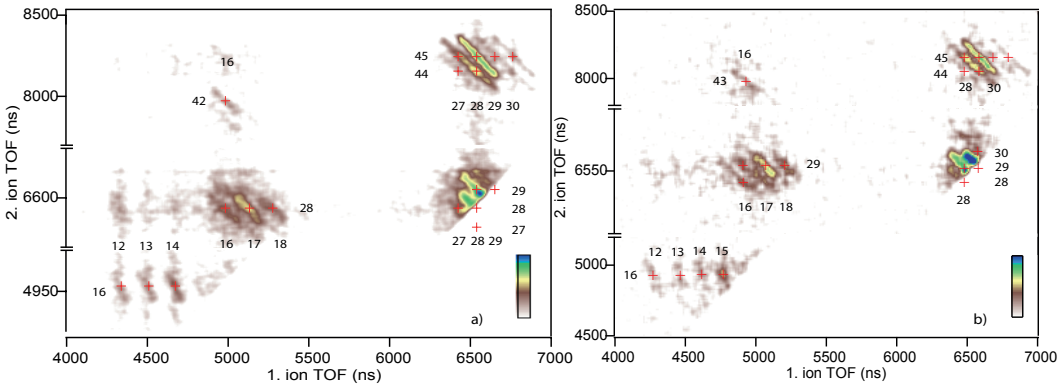

Figure 4: PEPIPICO maps of glycine (a) and ^{13}C-glycine (b).

Table I: Possible fragment coincident cations of glycine dication. Fragments in bold are the ones giving the major contribution, k denotes slope value and the column "Process" refers to Fig. 2 (see also Fig 5).

Masses	Fragment1	Fragment2	k_{exp}	k_{calc}	KER (eV)	Process	Masses	Fragment1	Fragment2	k_{exp}	k_{calc}	KER (eV)	Process
12, 16	$\mathbf{C^+}$	$\mathbf{O^+}$	-2.36±0.87	-2.42	4.5±0.4	(e)	16, 42	$\mathbf{O^+}$	$\mathbf{C_2NH_4^+}$	-1.04±0.18	-1.00		(c)
		NH_2^+							$C_2OH_2^+$				
13, 16	$\mathbf{CH^+}$	$\mathbf{O^+}$	-1.96±0.48	-2.23	4.3±0.4	(e)		NH_2^+	$C_2OH_2^+$				
		NH_2^+					27, 28	$\mathbf{CNH^+}$	$\mathbf{CO^+}$		-1.07		(e)
14, 16	$\mathbf{CH_2^+}$	$\mathbf{O^+}$	-1.73±0.45	-2.07	3.9±0.4	(e)	28, 28	$\mathbf{CNH_2^+}$	$\mathbf{CO^+}$	-1.07±0.19	-0.97	5.3±0.2	(e)
		NH_2^+					28, 29	$\mathbf{CNH_2^+}$	$\mathbf{COH^+}$	-1.00±0.28	-0.94	3.3±0.3	(e)
	N^+	O^+						CO^+	CNH_3^+				
16, 28	$\mathbf{NH_2^+}$	$\mathbf{CO^+}$	-1.15±0.28	-0.86	3.3±0.3	(d)	29, 29	$\mathbf{CNH_3^+}$	$\mathbf{COH^+}$	-1.06±0.17	-0.97		(e)
	O^+	CO^+					27, 44	$\mathbf{CNH^+}$	$\mathbf{CO_2^+}$		-1.09		(d)
		CNH_2^+					27, 45	$\mathbf{CNH^+}$	$\mathbf{CO_2H^+}$	- 1.00±0.18	-1.11		(b)
17, 28	$\mathbf{OH^+}$	$\mathbf{CNH_2^+}$	-1.00±0.10	-0.97	2.0±0.2	(b)	28, 44	$\mathbf{CNH_2^+}$	$\mathbf{CO_2^+}$	-0.93±0.22	-1.05		(d)
		CO^+					28, 45	$\mathbf{CNH_2^+}$	$\mathbf{CO_2H^+}$	-1.04±0.11	-1.07	6.0±0.2	(b)
18, 28	$\mathbf{H_2O^+}$	$\mathbf{CNH_2^+}$	-0.77±0.22	-0.97	1.6±0.2	(b)	29, 45	$\mathbf{CNH_3^+}$	$\mathbf{CO_2H^+}$	-1.00±0.17	-1.03		(b)
		CO^+					30, 45	$\mathbf{CNH_4^+}$	$\mathbf{CO_2H^+}$	-0.97±0.14	-1.00		(a)

illustrated in Fig. 5. Water is usually eliminated as a neutral molecule, but also water cation ejection is observed. **As glycine has several conformations in the gas phase where there is a hydrogen bond between hydroxyl (OH) and the amine (NH_2) groups (Fig. 1 (b) and (c)), we suggest that water elimination (process (b) of Fig. 5) is more prevalent in this kind of conformations. Furthermore, the ratio between the combined intensity of the fragmentation patterns corresponding to those processes involving water elimination is roughly 50% (or slightly less) of the total intensity of all the patterns. This is surprisingly well in line with the ratio (38.6%) of those conformations where the hydroxyl and amine groups are in the same side of the C-C_α bond (conformation (b) and (c) of Fig. 1).** Our interpretation concerning water elimination is also supported by the calculations concerning singly charged glycine; the interaction between the hydrogen atoms of NH_2 and the O atoms of the COOH moiety was found to be stronger in the case of ionized glycine compared to neutral glycine[11]. For the sake of simplicity, only conformer (b)/(c) of Fig. 1 has been used in Figure 5 and in all

Figures from here on. Note also that when a process is accompanied by hydrogen elimination, it was not possible to determine from the PEPIPICO analysis, at which stage of the dissociation it occurs (although it is tentatively associated to a specific step in Fig. 5), since the involved change of mass and PEPIPICO slope is too small.

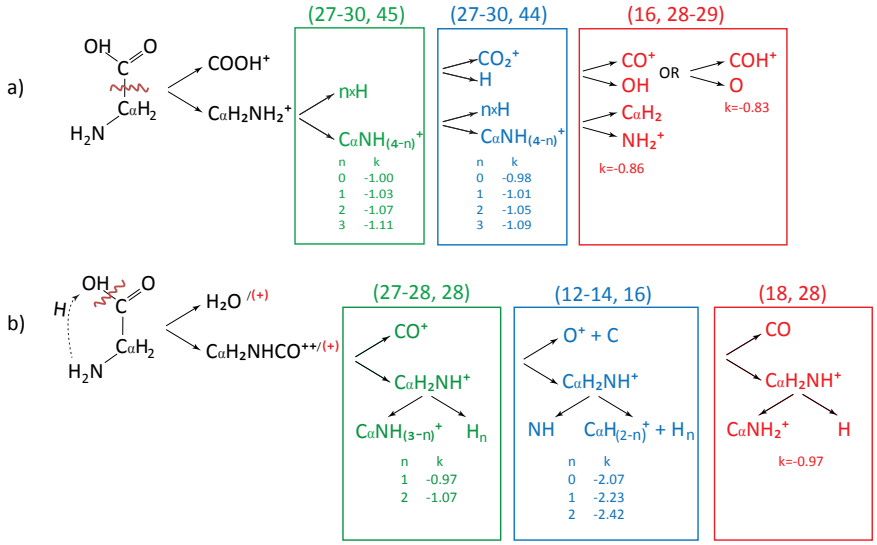

Figure 5: Fragmentation pathways of C 1s core-ionized glycine leading to different pairs of cations. (a) shows those pathways characterized by the C-C_α bond cleavage and (b) shows those pathways where also water elimination takes place.

1. *Fragmentation with primary rupture of C-C_α bond*

There are three different observed fragmentation channels that begin by a C-C_α bond rupture as seen from Fig. 5 (a). The heavy coincident ions follow fragmentation pathways ending with the fragments as shown in the two left frames (green and blue) in Figure 5 (a). As seen from Fig. 4, the pure two-body process is quite rare (the pattern corresponding to (30, 45) is very weak). Instead, the two strongest channels are those producing ion pairs corresponding to masses (28, 45) (*secondary decay* process) and (28, 44) (*two-step four-body secondary decay* process). In both cases the $C_\alpha NH_2^+$ fragment with mass 28 is created (which, as one soon notices, is also the case with other strong fragmentation channels). The calculated slope values of the processes are in good agreement with the experimental values as seen in Table I. Also the KER value of the ($C_\alpha NH_2^+$, $COOH^+$) pair is reasonable; the distance between the two positive charges at the moment of charge separation given by Eq. 3 is 2.4 Å, which fits well to the geometry of neutral and cationic glycine[11].

In the case of processes with large KER, the Equation 3 gives a good approximation for the distances between the

charges at the beginning of the charge separation. For processes having low KER (<3 eV), the distance given by Eq. 3 is unrealistically large. This is likely due to the lack of strong momentum correlation between the charged fragments; a notable portion of the kinetic energy released in the fragmentation process goes to the neutral fragment(s). This can also be seen as blurred patterns in the PEPIPICO map.

Unlike the other fragmentation channels beginning by the C-C_α bond rupture, the right (red) in Fig. 5 (a) produces only weak patterns. These patterns correspond to (16, 28) and (16, 29); no pattern change when comparing the PEPIPICO maps of glycine and ^{13}C-substituted glycine (Fig. 4). The coincident ion pairs must therefore be (NH_2^+, CO^+) and (NH_2^+, COH^+). Due to the weakness of this fragmentation channel, only slope value for the pattern corresponding to (16, 28) could be reliably determined, no KER value can be extracted. The experimental and calculated slope values, however, agree well.

2. Fragmentation with water cation elimination

As already mentioned, we propose that fragmentation processes involving water elimination are due to the conformations (b) and (c) of Fig. 1. The conformation (c) is clearly the most suitable for the starting point of fragmentation processes of Fig. 5 (b), but as fragmentation processes following core ionization and the subsequent Auger decay commonly involve atomic rearrangements, the processes of Fig. 5 (b) can essentially begin from any other conformation also.

Like in the case of C-C_α bond cleavage, also water elimination is involved in three fragmentation channels (see Fig. 5 (b)). The process described in the left frame is a strong fragmentation channel producing ion pairs with masses (27, 28) and (28, 28) in the case of glycine and (28, 28) and (29, 28) in the case of ^{13}C-glycine, therefore the ion pairs are ($C_\alpha NH^+$, CO^+) and ($C_\alpha NH_2^+$, CO^+). The one containing the $C_\alpha NH_2^+$ fragment is clearly stronger channel (see Fig. 4). The fragmentation processes are combinations of *deferred charge separation* and *secondary decay* where one of the coincident fragments always originates from the carboxyl radical (COOH). The KER of 5.3 eV corresponds to a distance of 2.7 Å between the two positive charges at the moment of charge separation when CO^+ and $C_\alpha H_2 NH^+$ ions are produced (see Fig. 5 (b)). This is a very realistic value, since the (calculated) bond distances in neutral and cationic glycine are in the range of 1.5 Å[11].

The three PEPIPICO patterns corresponding to masses (12-14, 16) are weak are likely produced as a result of a fragmentation pathways shown in Fig. 5 (b) (middle frame). As one can see from Table I, there are several possible

assignments for these fragments. The existence of N^+ in the case of (14, 16) can be excluded, because no reasonable fragmentation channel would produce this fragment with the detected pattern slope k= −1.73. Also, based on past experience it is unlikely that only N^+ from the amine group would appear in the pair while NH^+ and NH_2^+ are missing. For the same reason, O^+ is more plausible as the heavier fragment than NH_2^+. As there are four patterns instead of three on the map of ^{13}C-glycine (Fig 4 (b)) corresponding to masses (12-15, 16) it is clear that the cationic carbon can also originate from the COOH moiety.

The observed KERs (4.5 eV-3.9 eV) of these channels correspond to charge distances from 3.7 to 3.2 Å. These are a bit large values, but still realistic. This is so, because prior to charge separation the glycine molecule has fragmented into H_2O and $C_\alpha H_2NHCO^+$, which may well have more linear geometry than neutral glycine. In that case the charges at the moment of charge separation would be located to the opposite ends of $C_\alpha H_2NHCO^+$ leading to the observed KERs - although this is but a very rough indication of the electron density distribution.

The fragmentation process corresponding to pattern (18, 28) is the only one that involves water cation elimination. Because the pattern is shifted to (18, 29) in the case of ^{13}C-Glycine, the heavy fragment must be $C_\alpha NH_2^+$ and the fragmentation process is presented in Fig. 5 (b) (right frame). This pathway differs from the process of Fig. 5 (b) (left frame) producing the ($C_\alpha NH_2^+$, CO^+) pair only by charge location. In the case of neutral water elimination, the charge separation takes place in the second step of the fragmentation, whereas in the case of cationic water production it takes place in the first step. This leads to a much smaller KER (1.6 eV) compared to neutral water elimination and the production of CO^+ in coincidence with $C_\alpha NH_2^+$, with KER of 5.3 eV. Also, the PEPIPICO pattern of (H_2O^+, $C_\alpha NH_2^+$) is much more diffuse compared to that of ($C_\alpha NH_2^+$, CO^+), which implies that the momentum correlation between the H_2O^+ and CNH_2^+ is not that strong and a notable portion of the kinetic energy released during the dissociation goes to the neutral fragment(s). Hence also the KER assigned only to the charged fragments only, becomes smaller.

3. Other cases

In addition to fragmentation processes involving C-C_α bond cleavage and water elimination, there are two "special" cases that are not described in Fig. 5 and are presented in Fig. 6. The fragmentation channel Fig. 6 (a) produces patterns corresponding to (28, 29) and (29, 29) [(29, 29) and (30, 29) in the case of ^{13}C-Glycine], leading to assignments ($C_\alpha NH_2^+$, COH^+) and ($C_\alpha NH_3^+$, COH^+), respectively. The fragmentation processes are, like in Fig. 5 (b) (left frame),

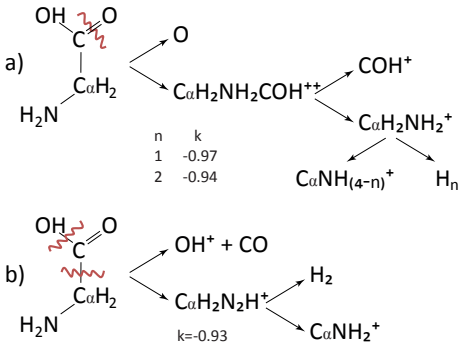

Figure 6: Fragmentation channels producing the patterns corresponding to masses (28-29, 29) and (17, 28).

also combinations of *deferred charge separation* and *secondary decay* where one of the coincident fragments always originates from the carboxyl radical (COOH). If the fragment from the $COOH^+$ is CO^+, neutral water elimination from the rest of the molecule takes place. In the case of COH^+ production, the fragmentation pathway is that of Fig. 6 (a). The most probable coincident ion for both CO^+ and COH^+, is $C_\alpha NH_2^+$.

The channel presented in Fig. 6 (b) produces only one PEPIPICO pattern, that corresponds to (17, 28) [(17, 29) in the case of ^{13}C-Glycine]; the heavier coincident fragment must unambiguously be $C_\alpha NH_2^+$ whereas the lighter fragment is probably OH^+. The fragmentation process is very similar to that of Fig. 5 (a) (left frame) producing the $C_\alpha NH_2^+$ and $COOH^+$ coincident fragments, except that in the case of (OH^+, $C_\alpha NH_2^+$) the COOH moiety breaks up in the first step of the fragmentation.

Both cases of Fig. 6 produce quite broad patterns as seen from Fig. 4, again indicating that a notable portion of the kinetic energy goes to the neutral fragment(s), and consequently KER from the charged particles is rather low. However, the calculated and experimental slope values agree quite well (see Table I), suggesting that the momentum correlation between the charged fragments is mostly retained.

Lastly, a separate vague and weak pattern, namely (16, 42) can be assigned to (O^+, $C_2NH_4^+$).

4. Fragmentation with proton ejection

As mentioned in the Introduction, fragmentation of core-ionized glycine is characterized by enhanced proton ejection. PEPIPICO maps showing patterns of fragments in coincidence with H^+ are presented in Fig. 7, which has been extracted from the ^{13}C-glycine data. Because of the high velocity of protons, the patterns can be incomplete due to

the collection efficiency considerably less than 100% and one cannot reliably determine the slope nor KER from the PEPIPICO data. The ions in coincidence with H^+ are those that are also detected in coincidence with other heavier

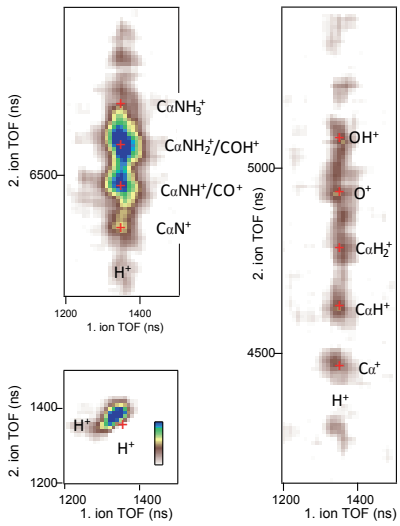

Figure 7: PEPIPICO map of ^{13}-glycine containing ion fragments in coincidence with H^+. The color scale indicating the pattern intensity is comparable with that of Fig, 4.

fragments, apart from the CN^+ fragment which only appears in coincidence with H^+. The strongest pairs are (H^+, H^+), (H^+, $C_\alpha NH^+$), (H^+, CO^+), (H^+, $C_\alpha NH_2^+$), (H^+, COH^+); all the heavy fragments are those also commonly present in the above discussed strong fragmentation channels. Similarly, the $C_\alpha N^+$ $C_\alpha NH^+$, $C_\alpha NH_2^+$, CO^+, COH^+ and $C_\alpha NH_3^+$ fragments produce weak patterns in coincidence with H^+ as is also the case with fragments with M>1. It has been noted throughout the text that the strongest fragmentation channels very often involve the production of the $C_\alpha NH_2^+$ fragment. This is the case with proton ejection too; comparison between normal and ^{13}C-labeled samples reveals that the strongest pair is (H^+, $C_\alpha NH_2^+$).

IV. CONCLUSIONS

Core ionization induced fragmentation of glycine is mainly governed by the rupture of C-C_α bond as is the case with valence ionization of glycine[23,25] and has been observed for core-ionized methionine too[33]. The fragmentation is characterized by two roughly equally common processes, where:

(a) coincident cations are formed as a result of the C-C_α bond cleavage (ion fragments with M>1 amu) or

(b) one of the coincident fragments is H^+ (proton creation).

In the case of (b), it is impossible to say where the charges are localized before the charge separation takes place, unlike in the case of (a), which seems to involve the localization of the positive charges to the opposite sides of the C-C_α bond. This might sound reasonable from the viewpoint of Coulomb repulsion, but one should not think that C-C_α bond is some kind of a barrier over which the charges do not easily move. The valence orbitals (also in the dicationic state of glycine) on where the electrons are located, are most likely delocalized over, if not the whole, at least most of the molecule. The final ion fragments are determined by the Auger final state following the initial core hole creation, not by Coulombic forces. The reason why the large coincident cations originate from the opposite sides of the C-C_α bond lies in the structure of the glycine molecule. Previous studies on fragmentation of core ionized molecules show that organic species often follow fragmentation pathways leading to well known stable cations such as CH_3^+ OH^+, $HNCH^+$, CO^+, COH^+ *etc*[36–39]. Furthermore, the final fragments often originate from different functional groups within the molecule as is essentially the case here too; one coincident ion comes from the CH_2NH_2 group and another from the COOH group of the glycine molecule.

Also water elimination during the fragmentation is characteristic for glycine. The results obtained here seem to indicate that those conformers where there is a hydrogen bonding between the hydroxylic and the amine groups lead to fragmentation processes involving water elimination. It thus seems that different conformers lead to different fragmentation channels or at least the ratios between different fragmentation channels depend on the initial conformation. In order to further lighten this matter, detailed calculations concerning the geometries of singly and doubly ionized glycine would be very beneficial.

The most abundant charged fragment in our study originates from the $C_\alpha H_2NH_2$ moiety as is also the case with valence ionization. The difference is that as valence ionization mainly produces $C_\alpha H_2NH_2^+$, core ionization favors $C_\alpha NH_2^+$. This is because in the case of valence ionization the amount of energy available for bond scissions is much lower than in the case of core ionization. Although $C_\alpha H_2NH_2^+$ is a stable ion, the fragmentation process here is so extreme that the $C_\alpha H_2NH_2$ is very rarely ejected as a $C_\alpha H_2NH_2^+$. Instead it gives up a number of neutral hydrogens, either as an H_2 (Fig. 5 (a)) or, if water elimination takes place, as an H (Fig. 5 (b)). The optimal number of donated hydrogens seems thus to be two. This is not that surprising because in the case of other nitrogen-containing organic molecules, core ionization often also leads to CNH_2^+ (or $HNCH^+$) production[32,36]. Note that CNH_2 is also known as a isolated species, methylene amidogen, found for example in interstellar space[40].

Lastly comparing the fragmentation of core-ionized glycine and methionine[33], an amino acid with notably longer

side-chain R, we find several similarities as well as differences. Similarly to glycine, methionine fragments via C-C_α bond cleavage producing most commonly the CNH_2^+ cation. Because the side-chain R ($CH_2CH_2SCH_3$) of methionine is replaced by H in the case of glycine, we can also mark the (H^+, CNH_2^+) pair of glycine as (R^+, CNH_2^+). In the case of methionine no corresponding fragment pair exists. In fact, in the case of core-ionized methionine, the R^+ ($CH_2CH_2SCH_3^+$) is not formed at all[33]. This raises a question of whether its length or the presence of the S atom in the side chain of methionine prevents the formation of R^+. In order to answer this question, we plan to investigate amino acids with side-chains that (a) have the same length as in methionine, but do not contain S, (b) are shorter than in methionine and (c) are shorter than in methionine and do not contain S.

Acknowledgements

Financial support from the Academy of Finland, the EU Transnational Access to Research Infrastructures programme, from the Graduate School of Materials Research and The National Doctoral Programme in Nanoscience of the Ministry of Education of Finland is acknowledged. M.A.H. acknowledges funding from the Natural Science and Engineering Council of Canada and the Canadian Space Agency. E.R. acknowledges funding from the Swedish Research Council (VR). The authors thank the staff of MAX-lab for their help during the experiments and express their gratitude to the Electron Spectroscopy Group of the University of Oulu for the opportunity to share their experimental equipment.

---

[1] Y.-J. Kuan, S.B. Charnley, H.-C. Huang, W.-L. Tseng, Z. Kisiel, Astrophys. J. **593**, 848 (2003).

[2] J. G. Lawless, Geochim. Cosmochim. Ac. **37**, 2207 (1973).

[3] Z. Martins, O. Botta, M. L. Fogel, M. A. Sephton, D. P. Glavin, J. S. Watson, J. P. Dworkin, A. W. Schwartz, P. Ehrenfreund, Earth Planet. Sci. Lett. **270**, 130 (2008).

[4] S. Pilling, D. P. P. Andrade, R. B. de Castilho, R. L. Cavasso-Filho, A. F. Lago, L. H. Coutinho, G. G. B. de Souza, H. M. Boechat-Roberty, A. Naves de Brito, Organic Matter in Space (IAU S251), (2008), p. 371.

[5] M.B. Simakov, E.A. Kuzicheva, A.E. Antropov, N. Ya Dodonova, Adv. Space Res. **30**, 1489 (2002).

[6] M. B. Simakov, Earth Planets Space **60**, 7582, (2008).

[7] G. Junk, H. Svec, J. Am. Chem. Soc. **85**, 839 (1963).

[8] I. D. Reva, A. M. Plokhotnichenko, S. G. Stepanian, A. Yu. Ivanov, E. D. Radchenko, G. G. Sheina, Y. P. Blagoi, Chem. Phys. Lett. **232**, 141 (1995).

[9] M. Noguera, L. Rodríguez-Santiago, M. Sodupe, J. Bertran, J. Mol. Struc-Theochem. **537**, 307 (2001).

[10] W. Wang, X. Pu, W. Zheng, N.-B. Wong, A. Tian, Chem. Phys. Lett. **370**, 147 (2003).

[11] S. Simon, A. Gil, M. Sodupe, J Bertrán, J. Mol. Struc-Theochem. **727**, 191 (2005).

[12] M.L. Gordon, G. Cooper, T. Araki, C. Morin, C. C. Turci, K. Kaznatcheev, A. P. Hitchcock, J. Phys. Chem A **107**, 6144 (2003).

[13] P. D. Godfrey, R D. Brown, J. Am. Chem. Soc. **117**, 2019 (1995).

[14] C. T. Falzon, F. Wang J. Chem. Phys. **123**, 214307 (2005).

[15] J. J. Neville, Y. Zheng, C. E. Brion, J. Am. Chem. Soc. **118**, 10533 (1996).

[16] C. J. Danby, J. H. D. Eland, Int. J. Mass Spectrom. and Ion Phys. **8**, 153 (1972).

[17] M. Simon, T. LeBrun, P. Morin, M. Lavolle, J.L. Marchal, Nucl. Instr. Methods B **62**, 167 (1991).

[18] L. J. Frasinski, M. Stankiewicz, K. J. Randall, P. A. Hatherly, K. Codling J. Phys. B **19**, L819 (1986).

[19] C. Harada, S. Tada, K. Yamamoto, Y. Senba, H. Yoshida, A. Hiraya, S. Wada, K. Tanaka, K. Tabayashi, Rad. Phys. Chem. **75**, 2085 (2006).

[20] J. H. D. Eland, Laser Chem. **11**, 259 (1991).

[21] E. Itälä, E. Kukk, D. T. Ha, S. Granroth, A. Caló, L. Partanen, H. Aksela, S. Aksela; J. Chem. Phys. **131**, 114314 (2009).

[22] E Kukk, G Prümper, R Sankari, M Hoshino, C Makochekanwa, M Kitajima, H Tanaka, H Yoshida, Y Tamenori, E Rachlew, K Ueda, J. Phys. B **40**, 3677 (2007).

[23] H-W. Jochims, M. Schwell, J-L. Chotin, M. Clemino, F. Dulieu, H. Baumgärtel, S. Leach, Chem. Phys. **298**, 279 (2004).

[24] V. S. Vukstich, A. I. Imre, L. G. Romanova, A. V. Snegursky, J. Phys. B **43**, 185208 (2010).

[25] A.F. Lago, L.H. Coutinho, R.R.T. Marinho, A. Naves de Brito, G.G.B. de Souza, Chem. Phys. **307**, 9 (2004).

[26] S. Maclot, M. Capron, R. Maisonny, A. Lawicki, A. Méry, J. Rangama, J-Y. Chesnel, S. Bari, R. Hoekstra, T. Schlathölter, B. Manil, L. Adoui, P. Rousseau, B. A. Huber, Chem. Phys. Phys. Chem. **12**, 930 (2011).

[27] S. Bari, F. Alvarado, J. Postma, P. Sobocinski, R. Hoekstra, T. Schlathölter, Eur. Phys. J. D **51**, 81 (2009).

[28] E. Kukk, R. Sankari, M. Huttula, A. Sankari, H. Aksela and S. Aksela, J. Electron Spectrosc. Relat. Phenom. **155**, 141 (2007).

[29] M. Huttula, S. Heinäsmäki, H. Aksela, E. Kukk and S. Aksela, J. Electron Spectrosc. Relat. Phenom. **156-158**, 270 (2007).

[30] V. Myrseth, J.D. Bozek, E. Kukk, L.J. Sæthre, T.D. Thomas, J. Electron Spectrosc. Relat. Phenom. **122**, 57 (2002).

[31] M. Bässler, A. Ausmees, M. Jurvansuu, R. Feifel, J.-O. Forsell, P. de Tarso Fonseca, A. Kivimäki, S. Sundin, S.L. Sorensen, R. Nyholm, O. Björneholm, S.Aksela, S. Svensson, Nucl. Instrum. Methods in Phys. A **469**, 382 (2001).

[32] E. Itälä, D. T. Ha, K. Kooser, E Nõmmiste, U. Joost, E. Kukk, Int. J. Mass Spectrom. **306**, 82 (2011).

[33] D. T. Ha, Y. Wang, M. Alcamí, E. Itälä, K. Kooser, S. Urpelainen, M. A. Huels, E. Kukk, F. Martín, J. Phys. Chem. A. **118**, 1374 (2013) .

[34] O. Plekan, V. Feyer, R. Richter, M. Coreno, M. de Simone, K. C. Prince, V. Carravetta, J. Phys. Chem. A, **111**, 10998 (2007).

[35] E. Itälä, D.T. Ha, K. Kooser, M.A. Huels, E. Rachlew, E. Nõmmiste, U. Joost, E. Kukk, J. Electron Spectrosc. Relat. Phenom. **184**, 119 (2011).

[36] E. Itälä, D. T. Ha, K. Kooser, E. Rachlew, M. A. Huels, E. Kukk, J. Chem. Phys. **133**, 154316 (2010).

[37] E. Itälä, M. A. Huels, E. Rachlew, K. Kooser, T. Hägerth, E. Kukk, J. Phys. B. **46**, 215102 (2013).

[38] E. Cortés, M. F. Erben, M. Geronés, R. M. Romano, C. O. Della Védova, J. Phys. Chem. A **113**, 564 (2009).

[39] J. H. D. Eland, B.J. Treves-Brown, Int. J. Mass Spectrom. and Ion Proc. **113**, 167 (1992).

[40] M. Ohishi, D. McGonagle, W. M. Irvine, S. Yamamoto, S. Saito, Astrophys. J. **427**, L51-4 (1994).

Appendix

There are two different three-body dissociation processes with general relationship between the fragmentation mechanism and the slope value: *secondary decay* and *deferred charge separation*. Deferred charge separation is a two-step process with the ejection of a neutral fragment from the doubly charged ion before the charge separation. Since the kinetic energy release in the first step is usually much smaller than during the charge separation, the two fragment ions have highly correlated momenta also in a deferred charge separation process, producing a PEPIPICO pattern with the slope $\approx k-1$ and KER as in the two-body case. One should note, that deferred charge separation can virtually be any n-body process; the same equations still stand no matter how many neutral fragments eject before the charge separation.

In secondary decay process, the charge separation occurs in the first step, after which the ejection of a neutral particle by one of the charged particles takes place:

$$M^{2+} \rightarrow (M_0) + M_1^+ + M_2^+ \rightarrow (M_0) + M_1^+ + M_{2a}^+ + M_{2b}.$$

The M_0 denotes the possible neutral fragment release in the charge separation step. As the neutral M_0 fragment takes negligible kinetic energy, the slope can be expressed as:

$$k \approx -\frac{M_2}{M_{2a}}, \quad \text{if} \quad M_{2a} < M_1 \quad \text{and} \quad k \approx -\frac{M_{2a}}{M_2}, \quad \text{if} \quad M_{2a} > M_1.$$

(In the case of $M_{2a} = M_1$ patterns with both slopes are superimposed in the PEPIPICO map.) Here it is again assumed that the kinetic energy release in the neutral fragment ejection is comparatively small. In this case the

(approximate) momentum correlation is between fragments 1 and 2, but the length of the PEPIPICO pattern is defined by the detected ions 1 and 2a. The unseen neutral fragment also carries away some momentum that must be taken into account, so we have

$$v_2 \approx v_{2a} \approx v_{2b} \Rightarrow p_{2a} = m_{2a} \cdot v_{2a} \approx M_{2a}\frac{M_1}{M_2} \cdot v_1 = -\frac{M_{2a}}{M_2} \cdot p_1 = \frac{M_{2a}}{M_2} \cdot p_2.$$

The pattern length is thus:

$$W = \frac{2 \cdot s}{q \cdot U} \cdot \sqrt{p_1^2 + p_{2a}^2} \approx \frac{2 \cdot s}{q \cdot U} \cdot \sqrt{1 + \frac{M_{2a}^2}{M_2^2}} \cdot p$$

and the KER:

$$KER = p^2(\frac{1}{2M_1} + \frac{1}{2M_2}).$$

A combination of deferred charge separation and secondary decay (or a set of secondary decays) is also quite common. Let us consider a following process:

$$M^{2+} \rightarrow M_A + M_0^{2+} \rightarrow M_A + M_1^+ + M_2^+ \rightarrow M_A + M_1^+ + M_{2a}^+ + M_{2b}.$$

The kinetic energy of the neutral fragments is again assumed to be very small. The slope and KER values are determined as in case of secondary decay.

Last process described here is *two-step four-body secondary decay*, where the charge separation is followed by the ejection of a neutral particle from both singly charged ions process:

$$M^{2+} \rightarrow M_1^+ + M_2^+ \rightarrow M_{1a} + M_{1b}^+ + M_{2a} + M_{2b}^+.$$

The slope for this kind process is

$$k \approx -\frac{M_{2b}}{M_{1b}}\frac{M_1}{M_2}, \quad \text{if} \quad M_{2b} > M_{1b} \quad \text{and} \quad k \approx -\frac{M_{1b}}{M_{2b}}\frac{M_2}{M_1}, \quad \text{if} \quad M_{2b} < M_{1b}.$$

Now both unseen neutral fragments carry away some momentum that must be taken into account.

$$v_1 \approx v_{1a} \approx v_{1b} \Rightarrow p_{1a} \approx \frac{M_{1a}}{M_2} \cdot p_1,$$
$$v_2 \approx v_{2a} \approx v_{2b} \Rightarrow p_{2a} \approx \frac{M_{2a}}{M_2} \cdot p_2.$$

The pattern width is now

$$W = \frac{2 \cdot s}{q \cdot U} \cdot \sqrt{p_1^2 + p_{2a}^+} \approx \frac{2 \cdot s}{q \cdot U} \cdot \sqrt{\frac{M_{1a}^2}{M_1^2} + \frac{M_{2a}^2}{M_2^2}} \cdot p$$

and the KER:

$$KER = p^2(\frac{1}{2M_1} + \frac{1}{2M_2}).$$